Journal of Physics and Chemistry of Solids 71 (2010) 314–322

Contents lists available at ScienceDirect

Journal of Physics and Chemistry of Solids

journal homepage: www.elsevier.com/locate/jpcs

Optical properties of the alkali antimonide semiconductors Cs_3Sb, Cs_2KSb, CsK_2Sb and K_3Sb

L. Kalarasse, B. Bennecer *, F. Kalarasse

Physics Laboratory at Guelma, Faculty of Science and Engineering, University of Guelma, P.O. Box 401, Guelma 24000, Algeria

ARTICLE INFO

Article history:
Received 16 February 2009
Received in revised form
22 December 2009
Accepted 25 December 2009

Keywords:
A. Semiconductors
C. Ab initio calculations
D. Optical properties

ABSTRACT

First principles calculations, by means of the full-potential linearized augmented plane wave method within the generalized gradient approximation, were carried out for the electronic and optical properties of the alkali antimonide compounds Cs_3Sb, Cs_2KSb, CsK_2Sb and K_3Sb. The calculated lattice parameters and bulk moduli are in good agreement with the available data. The calculated band structures and density of states are in good agreement with previous calculations. The peaks and structures in the optical spectra are assigned to interband transitions. The calculated absorption coefficient for K_3Sb and Cs_3Sb is in fairly agreement with the observed one.

1. Introduction

Alkali and bialkali antimonide are interesting semiconducting compounds, characterized by high quantum efficiency which makes them very suitable for technological applications as photodetectors and emitters. Since the earlier investigation [1–8], alkali antimonide compounds have attracted much attention and extensive experimental studies on their properties have been carried out [9–25].

However, little theoretical works have been devoted to the study of the electronic structure of alkali and bialkali antimonide compounds. The band structure have been calculated by empirical pseudopotential method and pseudopotential [11]. Christensen [26] have used the linear muffin tin orbitals method in the atomic sphere approximation (LMTO-ASA) to study the structural phase stability of a series of intermetallic compounds including the alkali antimonides. After that, Zunger and Wei [27] have performed a systematic study on the electronic structure using the full-potential linearized augmented plane wave method (FP-LAPW) and showed that the M_3^ISb ($M=Li, K, Cs$) compounds can be mapped to filled tetrahedral compounds (i.e., $(M_2^ISb)^-$ filled by M^{I+} ions), and discussed the main features of the electronic structure in terms of volume, p–d repulsion cation s and electrostatic (the interstitial insertion rule) effects. Recently, Ettema and de Groot [28–31] have studied the electronic structure of alkali and bialkali compounds using the localized spherical wave method (LSW) [28–30] and the FP-LAPW [31]. Unfortunately, up to now there is no theoretical work concerning their linear optical properties, despite their potential technological applications.

In this paper, we present studies of the linear optical properties of Cs_3Sb, Cs_2KSb, CsK_2Sb and K_3Sb compounds. The calculations are performed using the full potential linear augmented plane wave (FP-LAPW) method [32,33], in conjunction with the generalized gradient approximation (GGA) [34]. The features and structures of the obtained optical spectra are assigned to interband transitions along the Brillouin zone high symmetry lines.

The rest of this paper is organized as follows; in Section 2 we describe the method and we give the details of calculations; in Section 3 the obtained results are given and discussed. A conclusion is given in Section 4.

2. Crystal structure and computational details

The alkali compounds considered in this work crystallize in the DO_3 cubic structure (O_h^5 space group). The unit cell contains four formula units and represented by four face-centered sublattices shifted by $a\sqrt{3}/4$ along the body diagonal as illustrated in Fig. 1. The antimony atom occupy the first sublattice (the sites **a**). Two of the alkali atoms (M_{II}) occupy the second and fourth sublattices (the sites **c**) and the third alkali atom (M_I) occupy the third sublattice (the sites **b**). So that, there exist two different types of cations in this structure. The M_{II} with four cations and four anions as neighbors, and the M_I with eight M_{II} cations as neighbors.

The present calculations are performed using the full potential linear augmented plane wave method within the generalized

* Corresponding author. Tel.: +213 37 20 81 16; fax: +213 37 20 72 68.
E-mail address: b_bennacer@hotmail.com (B. Bennecer).

0022-3697/$ - see front matter © 2010 Elsevier Ltd. All rights reserved.
doi:10.1016/j.jpcs.2009.12.083

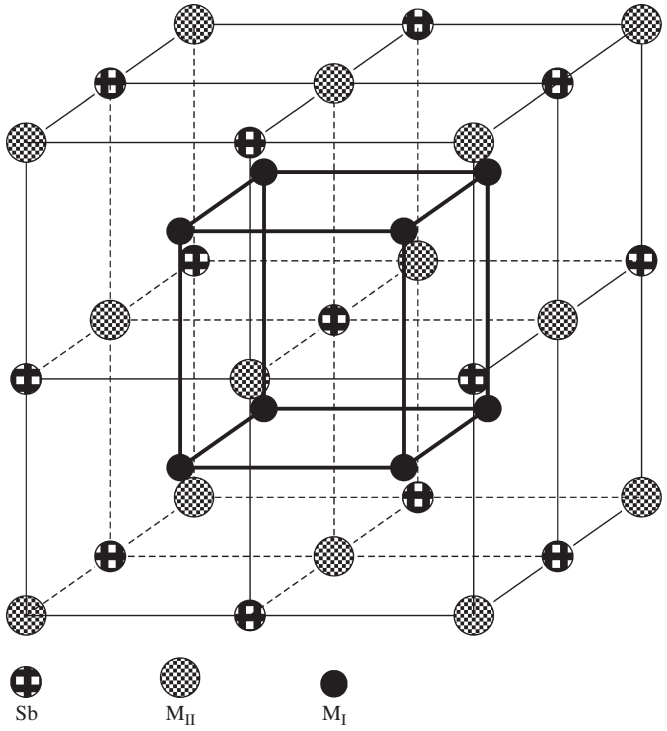

Fig. 1. The DO_3 crystal structure.

Table 1
Structural parameters, lattice parameter a_0 in (Å), bulk modulus B in (GPa), bulk modulus pressure derivative B' of Cs_3Sb, Cs_2KSb, CsK_2Sb and K_3Sb.

	This work	Other	Expt.
Cs_3Sb			
a_0	8.92	9.415[a], 9.15[b], 9.06[a]	9.128[a]
B	13.8314	15.1[a], 14[a]	
B'	4.136		
Cs_2KSb			
a_0	8.90		8.88[b]
B	12.59		
B'	3.79		
CsK_2Sb			
a_0	8.508		8.61[b,c]
B	14.8357		
B'	4.477		
K_3Sb			
a_0	8.42	8.357[a]	8.493[a]
B	13.203	14.8[a]	
B'	4.245		

[a] Ref. [27].
[b] Ref. [30].
[c] Ref. [8].

gradient approximation (GGA), as implemented in the Wien2k code [33]. In this method the space is divided into non-overlapping muffin-tin (MT) spheres separated by an interstitial region, in this context the basis functions are expanded in combinations of spherical harmonic functions inside the muffin-tin spheres and plane waves in the interstitial region. In this work we treat the core electrons fully relativistically, and the valence electron scalar relativistically (all the relativistic effects are taken into account except the spin–orbit coupling).

In the calculations, the K($3s^2 3p^6 4s^1$), Cs($4d^{10} 5s^2 5p^6 6s^1$) and Sb($4d^{10} 5s^2 5p^3$) states are treated as valence electrons, and the muffin-tin radii are chosen to be 2.5 Bohr for all atoms. The basis functions are expanded up to $R_{mt} \times K_{max} = 10$ (where K_{max} is the plane wave cut-off and R_{mt} is the smallest of all MT sphere radii), and up to $l_{max} = 10$ in the expansion of the non-spherical charge and potential. We use the Wu and Cohen functional [34] for the exchange and correlation interaction. For the integration we used $10 \times 10 \times 10$ k−points mesh in the whole first Brillouin zone and the self-consistent calculations are considered to be converged when the total energy is stable within 0.1 mRy.

The linear optical properties in solids can be described with the complex dielectric function $\varepsilon(\omega) = \varepsilon_1(\omega) + i\varepsilon_2(\omega)$, the inter-band contribution to the imaginary part of $\varepsilon(\omega)$ is calculated by summing transitions from occupied to unoccupied states over the Brillouin zone, weighted with the appropriate momentum matrix elements. In the present calculations the imaginary, or absorptive part of the dielectric tensor, is given by [35]

$$\mathrm{Im}\,\varepsilon(\omega) = \varepsilon_2(\omega) = \frac{4\pi^2 e^2}{m^2\omega^2} \sum_{i,j} \int |\langle i|M|j\rangle|^2 (f_i(1-f_j))\delta(E_f - E_i - \hbar\omega)\, d^3k \tag{1}$$

where e and m are the electron charge and mass, respectively, ω is the frequency of the photon, M is the momentum operator, $|i\rangle$ is the wave function, corresponding to eigenvalue E_i, and f_i is the Fermi distribution for $|i\rangle$ state. The integral over the Brillouin zone (BZ) was performed using the tetrahedron method. The calculated optical spectra depend strongly on the BZ sampling, therefore a sufficiently dense k-mesh is used in the calculations of optical spectra, which consists of $32 \times 32 \times 32$ k−mesh.

3. Results and discussion

3.1. Structural and electronic properties

The equilibrium structural parameters are determined by fitting the total energy as a function of volume to the Murnaghan's equation of state (eos) [36]. The structural parameters are listed in Table 1, in which the available experimental data and results of other calculations are also shown. The lattice parameters agree with the measured values within 2%. However, the lattice parameter of Cs_2KSb (8.90 Å), which has not been reported experimentally, is close to the one estimated by Ettema and de Groot (8.88 Å) [30]. Our bulk modulus values are slightly smaller than those reported by Christensen [26] and Wei and Zunger [27]. The bulk modulus pressure derivatives B' fall within the range 3–5 as it is the case for most solids.

The electronic band structures, density of states and optical spectra are calculated at the theoretical lattice constants. The calculated band structures and the corresponding total density of states (DOS) are shown in Figs. 2–5 for the studied compounds. Figs. 6–9 display the site and angular momentum decomposed density of states (PDOS). These results are in good agreement with previous calculations of Wei and Zunger [27] and Ettema and de Groot [28–30]. From these figures, the valence bands are dominated by Sb s and p states.

For Cs_3Sb, Cs_2KSb and CsK_2Sb, the lowest valence band is an Sb 5s state which is dispersionless and localized around −7 eV energy range, with a mixture of some Cs p states, the Cs contribution is more pronounced in Cs_3Sb and Cs_2KSb. The Sb p states with a more dispersion, spread between −1.2 and 0 eV with small hybridization with Cs p states.

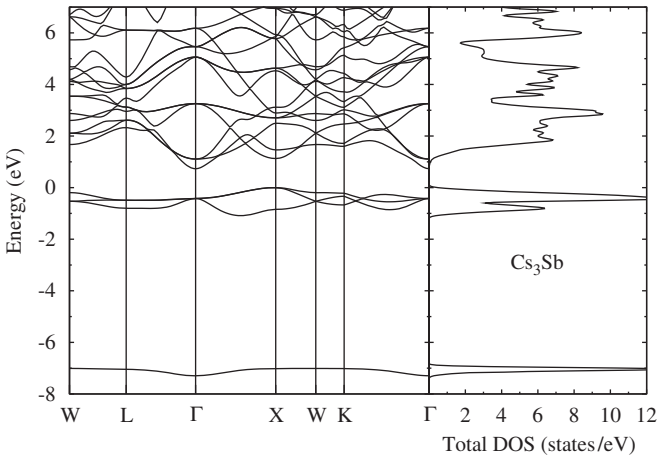

Fig. 2. Electronic band structure (left panels) and total density of states (right panels) for Cs_3Sb, the Fermi level is set to zero.

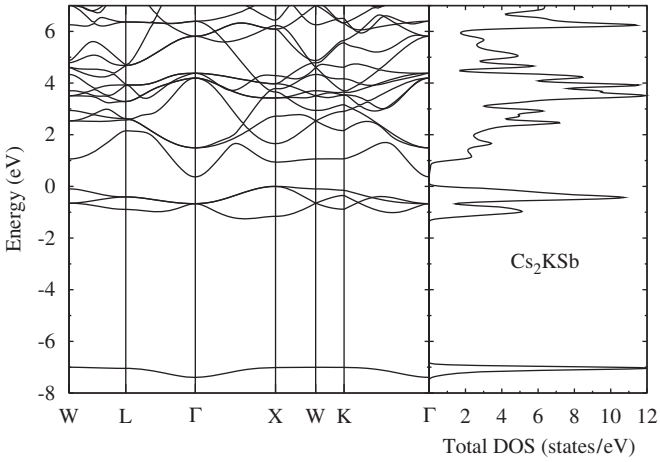

Fig. 3. As Fig. 2, but for Cs_2KSb.

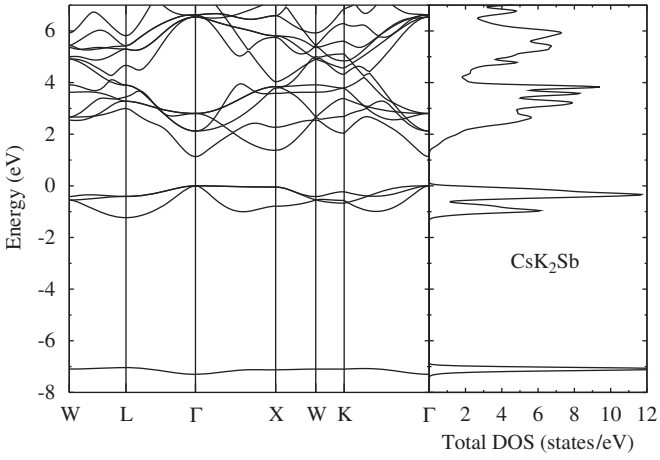

Fig. 4. As Fig. 2, but for CsK_2Sb.

For K_3Sb, the Sb s states are also localized around −7 eV energy range and mixed with small amount of K p states. The Sb p states are spread between −1 eV and 0 eV with a little hybridization with K p states, these top valence bands form the initial states in the photoabsorption process.

The conduction bands are a mixture of d, s and p orbitals. However, one has to note that the conduction band bottom at Γ is

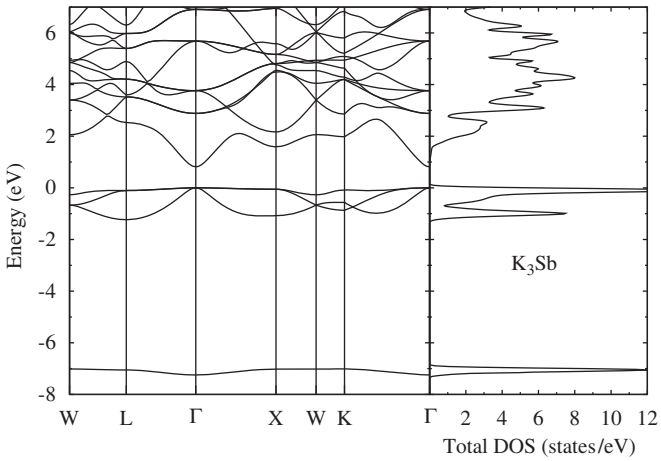

Fig. 5. As Fig. 2, but for K_3Sb.

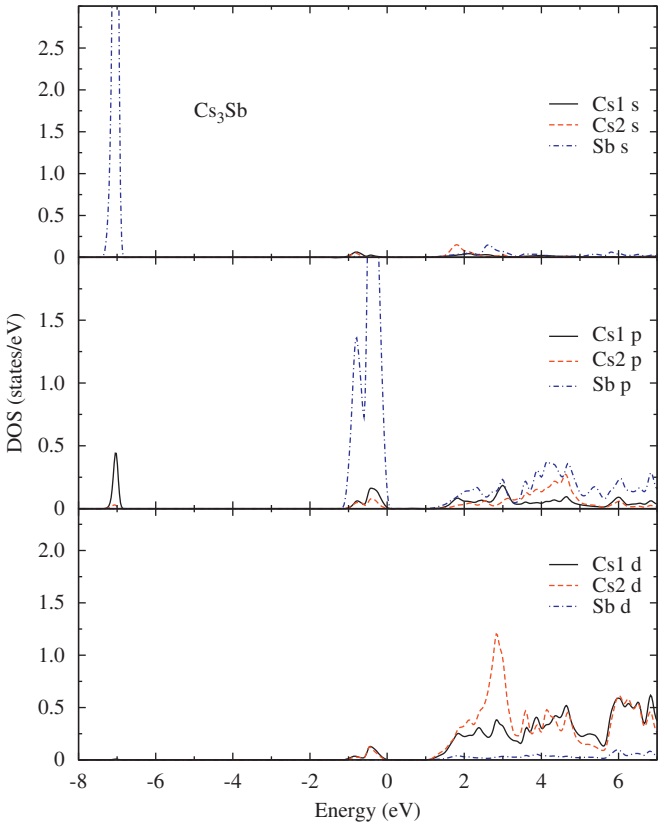

Fig. 6. Site and angular momentum decomposed DOS of Cs_3Sb, the Fermi level is set to zero.

due to the s states, see Table 2 where the *l*-decomposed charge characters inside the muffin-tin spheres at the high symmetry points Γ, L and X are displayed.

The main feature of the density of states is that the valence and the conduction bands are dominated by the Sb states. Similar results were obtained by Wei and Zunger [27] where they showed that the electronic structure of Cs_3Sb, K_3Sb and Li_3Sb are comparable with the hypothetical compound Sb^{-3} with the same lattice dimensions (i.e., each compound is compared with Sb^{-3} at the lattice parameter of that compound), their study indicates that the electronic structure is largely determined by the overlap of the Sb orbitals.

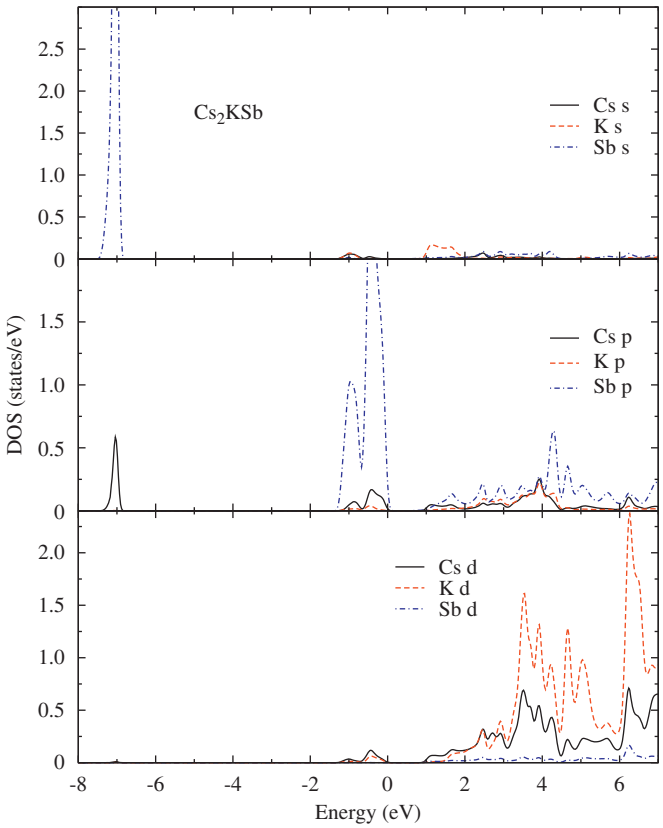

Fig. 7. As Fig. 6, but for Cs_2KSb.

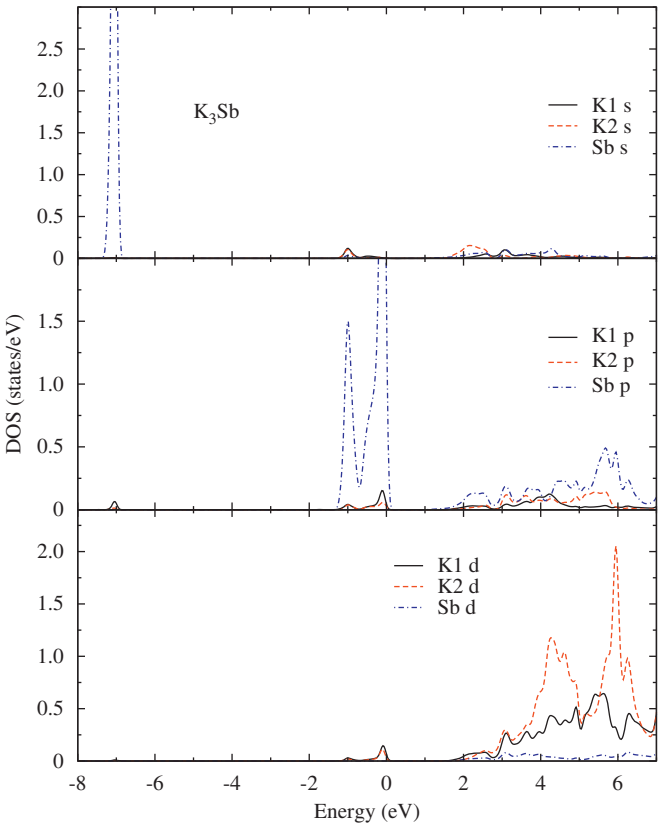

Fig. 9. As Fig. 6, but for K_3Sb.

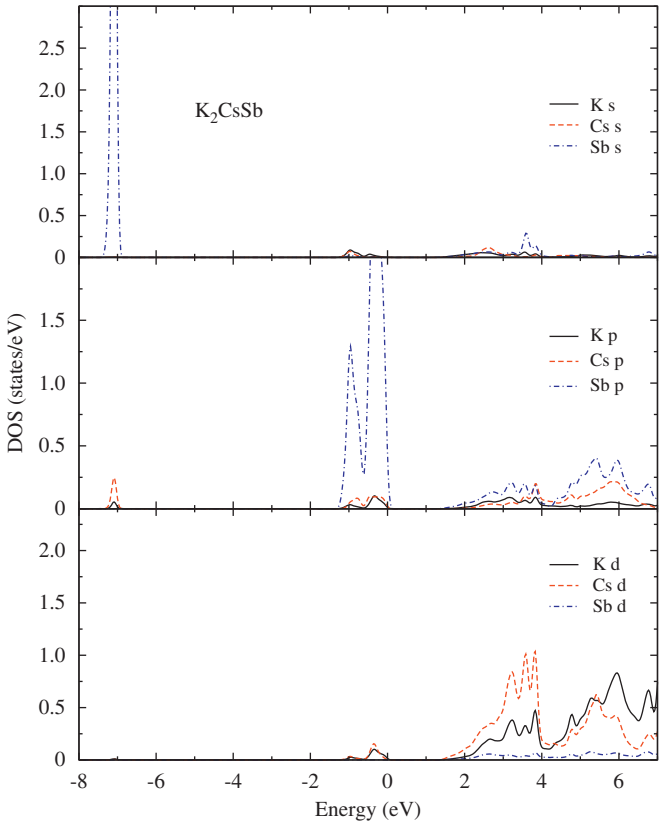

Fig. 8. As Fig. 6, but for CsK_2Sb.

Table 2
Calculated *l*-decomposed local charge character (in percentage) inside muffin-tin spheres in the first conduction band at high symmetry points.

Cs_2KSb			Cs_3Sb			K_2CsSb			K_3Sb		
s	p	d	s	p	d	s	p	d	s	p	d
Γ											
9.05	0.00	0.00	9.37	0.00	0.00	13.64	0.00	0.00	13.31	0.00	0.00
6.85	0.00	0.00	4.62	0.00	0.00	4.67	0.00	0.00	6.29	0.00	0.00
2.73	0.00	0.00	3.02	0.00	0.00	4.29	0.00	0.00	3.61	0.00	0.00
L											
0.00	8.05	0.00	0.00	0.32	0.00	4.84	0	1.26	6.31	0.00	0.93
6.63	0.00	2.65	2.69	0.00	8.22	0.00	6.65	0.00	0.00	3.69	0.00
0.03	0.51	4.17	0.17	0.54	4.64	5.10	0.60	0.19	4.42	0.77	0.15
X											
0.50	0.00	0.66	0.00	0.00	0.64	0.00	0.00	1.08	0.45	0.00	1.04
7.68	0.00	0.51	0.00	0.00	6.93	0.00	0.00	7.83	8.93	0.00	0.02
0.00	2.31	3.01	1.86	0.00	2.74	3.34	0	2.35	0.00	1.88	2.36

For each state the *l* characters are given for Sb (first row), M^{II} (second row) and M^{I} (third row).

The calculated bandgaps are listed in Table 3 together with the results of other calculations and the experimental values. As seen in this table, K_3Sb and CsK_2Sb have direct bandgap with the maximum of the valence band at the Γ point. However, for the other two compounds Cs_3Sb and Cs_2KSb the gap is indirect since the valence band maximum is at the X point whereas the minimum of the conduction band is at Γ point.

Table 3
Calculated and experimental bandgaps (eV) for Cs_3Sb, Cs_2KSb, CsK_2Sb and K_3Sb.

	Direct gap (Γ−Γ)		Direct gap (X−X)		Indirect gap (X−Γ)		Expt.
	This work	Other	This work	Other	This work	Other	
Cs_3Sb	1.412	1.02 [27]	1.111		0.918	1.75 [27]	1.6 [17,24]
Cs_2KSb	1.152		0.945		0.460	0.58 [30]	
CsK_2Sb	1.13		1.419		1.333		1.2 [10]
K_3Sb	0.832	0.59 [28], 0.56 [27]	1.655		0.883	1.39 [27]	1.8 [10], 1.1 [17], 0.79 [28]

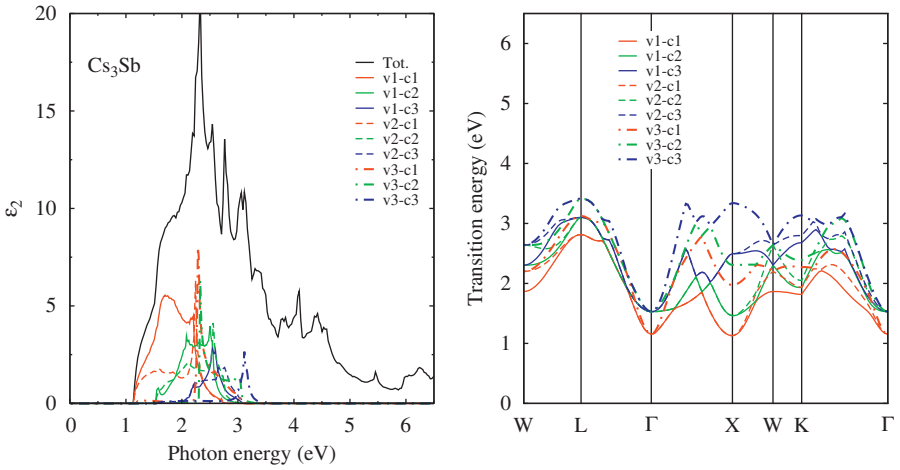

Fig. 10. The decomposition of the imaginary part of the dielectric function into band-to-band contributions (left panel) and the transition energy band structure (right panel) for Cs_3Sb. The counting of the bands is down (up) from the top (bottom) of the valence (conduction) band.

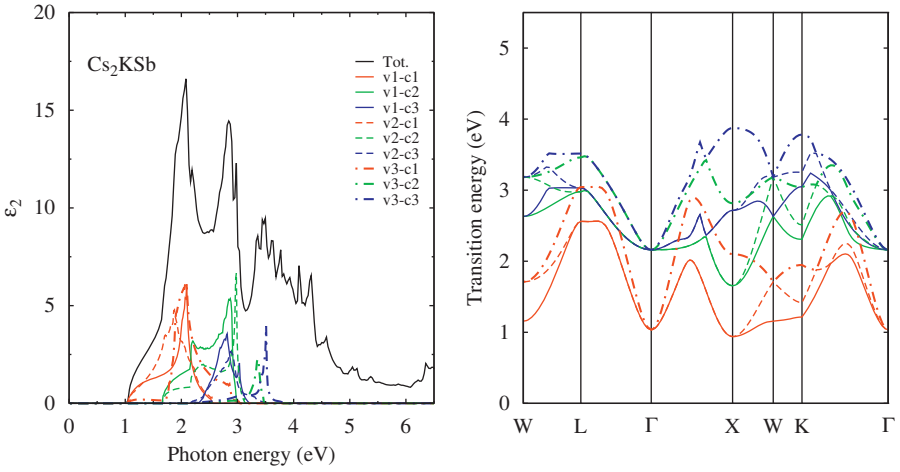

Fig. 11. As Fig. 10, but for Cs_2KSb.

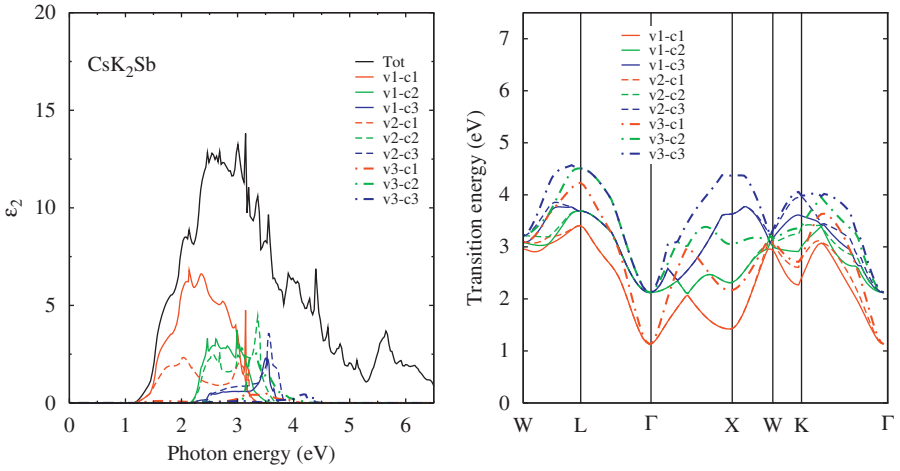

Fig. 12. As Fig. 10, but for CsK_2Sb.

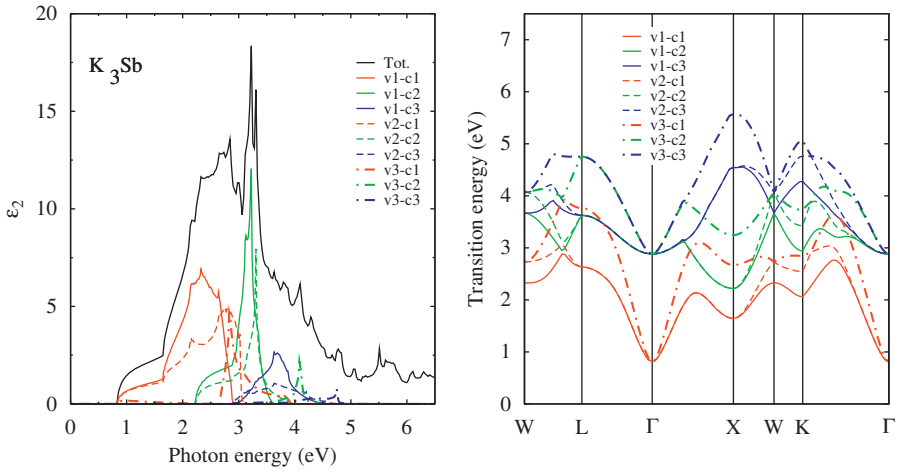

Fig. 13. As Fig. 10, but for K_3Sb.

One further point needs to be added is that the difference between the indirect and the direct gaps at Γ point for the former compounds, i.e., K_3Sb and CsK_2Sb, is smaller than those for the later ones, i.e., Cs_3Sb and Cs_2KSb.

The discrepancy between the calculated values of the gaps and the measured ones is due to the approximation used to evaluate the exchange and correlation interaction, i.e., GGA. In order to overcome this problem and obtain more realistic values for this quantity one should go beyond this approximation and use the GW one [37–43].

3.2. Optical properties

3.2.1. The dielectric function

The absorptive (imaginary) parts of the dielectric function ε_2 are displayed in Figs. 10–13 for the studied compounds. The analysis of the calculated optical spectra and the determination of the origins of the different peaks and features are performed on the basis of decomposing each spectrum to its individual pair contribution, i.e., contribution from each pair of valence vi and conduction cj bands (vi–cj), and plotting the transition (from valence to conduction) band structures, i.e., transition energy $E(k)=E_{cj}(k)-E_{vi}(k)$ (see Fig. 10 right panel for example). These techniques allow the knowledge of the bands which contribute more to the peaks and their locations in the Brillouin zone [44–47]. The positions of the peaks and the corresponding interband transition and their locations in the Brillouin zone are reported in Tables 4–7 for the studied compounds.

The different structures in the optical spectra of the studied compounds are due to the differences in their band structures. The main contribution to the optical spectra originates from the transitions from the top three valence bands to the lower three conduction bands. The details of the optical spectra are given below.

Cs_3Sb: The spectrum of Cs_3Sb is different from the others. The threshold in ε_2 at 1.11 eV is caused by the v_1-c_1 and v_2-c_1 transitions at X point which corresponds to the direct gap. The rise and shoulder in the energy range of 1.11–2 eV have four main contributions (i) the v_1-c_1 transition in the Γ–X–W–K regions and in the Σ line near Γ, (ii) the v_2-c_1 transition in the Δ line and at W point, (iii) the v_1-c_2 in Γ–X–W region and (iv) v_2-c_2 transition around Γ, X and K points. The main peak at 2.19 eV originates mainly from the v_2-c_1 transition in Σ line, v_3-c_1 in X–W–K region and v_3-c_2 transition at the K point. The rest of structures below 3.0 eV comes from the v_1-c_2, v_2-c_2 and v_2-c_3 transitions. The structures above 3 eV comes from the v_3-c_3 and v_3-c_1 transitions. The positions of the peaks and major contributions are listed in Table 4.

Table 4
Optical transitions in Cs_3Sb.

Peak position	Transition	Energy (eV)
1.86	(v_1-c_1) W, L–Γ, W–K–Γ, K	1.72, 1.74
	(v_2-c_1) L–Γ, X–W, K–Γ	1.83
2.08	(v_1-c_1) W–L–Γ, K–Γ	2.12
	(v_1-c_2) L–Γ, X–W–K–Γ	2.08, 2.12
	(v_2-c_2) L–Γ, X–W, K, K–Γ	2.08, 2.13
2.19	(v_1-c_1) W–L–Γ, K–Γ	2.16, 2.20
	(v_1-c_2) L–Γ, X–W–K–Γ	2.17
	(v_2-c_1) W, L–Γ, K–Γ	2.24
	(v_1-c_3) L–Γ–X, K–Γ	2.20
	(v_2-c_2) L–Γ, X–W–K	2.24
	(v_2-c_3) L–Γ–X, K–Γ	2.23
2.32	(v_1-c_2) W, L–Γ, K–Γ	2.31, 2.36
	(v_3-c_1) W, L–Γ–X, W–K–Γ, K	2.28
	(v_3-c_2) L–Γ–X, X, K–Γ	2.32
2.54	(v_1-c_2) W–L–Γ, K–Γ	2.50
	(v_1-c_3) W–L–Γ, X–W–K–Γ	2.54, 2.59
	(v_2-c_2) W, L–Γ, K–Γ	2.55
	(v_2-c_3) W, L–Γ, X, X–K–Γ, K	2.57, 2.65
	(v_3-c_1) W–L–Γ–X, K–Γ	2.58
2.76	(v_2-c_3) W–L–Γ, X–W–K–Γ, W	2.76, 2.69
	(v_3-c_2) W, W–L–Γ–X, K–Γ	2.85
3.06	(v_3-c_3) W–L–Γ, K–Γ	2.89, 2.96
3.11	(v_3-c_3) W–L–Γ	3.11

Cs_2KSb: The most striking features in this spectrum is the appearance of two pronounced peaks of almost the same height in the visible region and denser structure for photon energies higher than 3 eV. The first peak which is lower in intensity than the corresponding one in Cs_3Sb comes from the transition from the top three valence bands to the first conduction band. There are three main contribution to this peak: (i) v_1-c_1 in the Δ and Σ

lines, (ii) v_2-c_1 in the Δ line and (iii) v_3-c_1 in the X–W direction. The second peak originates from $v_1-c_{2,3}$ in the W–L directions. The structure for the photon energies greater than 3 eV (UV region) comes from $v_3-c_{2,3}$ transitions.

CsK_2Sb and K_3Sb: These two compounds have a direct gap at Γ point, which corresponds to the threshold in the imaginary part of the dielectric function. The hip at 2.08 eV for CsK_2Sb is due to v_1-c_1 transition in the Δ line as it is clear from the energy transition in the right panel of Fig. 12. For CsK_2Sb the structure in the energy range 2–3 eV originates from the v_1-c_1 in the X–W–K region and $v_{1,2}-c_2$ in X−Γ−W regions and the Σ line. While it originates from most regions except around Γ and X for the $v_{1,2}-c_1$ in K_3Sb. The main peak in the UV region comes from the v_1-c_2 transition in the Σ line. For photon energies higher than 3 eV the main contribution is from the $v_{2,3}-c_{2,3}$ transitions.

The experimental imaginary part of the dielectric function for the cubic K_3Sb was reported by Ebina and Takahashi [9]. It shows three peaks and a dip in between like our calculated spectrum. Their energy positions are close to the computed ones.

The dielectric constant: Like the fundamental gap, the static dielectric constant $\varepsilon(0)$ is a very important physical quantity for semiconductors. The real parts of the dielectric are calculated from the imaginary ones by using the Kramers–Kronig relation, but they are not shown here. We just report the values obtained for $\varepsilon(0)$. However, the underestimation of the gaps leads to the overestimation of $\varepsilon(0)$ [48,49]. This overestimation is corrected by allowing a constant energy shift for the conduction

Table 5
Optical transitions in Cs_2KSb.

Peak position	Transition	Energy (eV)
2.08	(v_1-c_1) W−L−Γ, K−Γ	2.09
	(v_2-c_1) W−L−Γ−X, K−Γ	1.88
	(v_3-c_1) W−L−Γ−X−W, X, K−Γ	2.08
	(v_1-c_2) Γ−X−W	2.20
2.84	(v_1-c_2) W−L−Γ, K−Γ	2.84, 2.87
	(v_1-c_3) W−L−Γ, X−W−K−Γ	2.81
	(v_2-c_3) L−Γ, X–W, K−Γ	2.88
	(v_3-c_1) W−L−Γ−X	2.85, 2.81
2.97	(v_2-c_2) W–L, L, X−W−K−Γ	2.97
	(v_1-c_3) W–L, L, W−K−Γ, K	3.03
3.36	(v_3-c_2) W−L−Γ−X, K−Γ	3.37
3.49	(v_3-c_3) W–L, L, Γ−X−W−K−Γ	3.51

Table 6
Optical transitions in CsK_2Sb.

Peak position	Transition	Energy (eV)
2.08	(v_1-c_1) L−Γ, X–W, K−Γ	2.095, 2.13
	(v_2-c_1) L−Γ, X–W, K−Γ	2.02
2.54	(v_1-c_1) L−Γ, X−W−K−Γ	2.35
	(v_1-c_2) L−Γ, X–W, K−Γ	2.46, 2.57
	(v_1-c_3) L−Γ−X, K−Γ	2.53
	(v_2-c_2) L−Γ, X–W, K−Γ	2.55
2.62	(v_1-c_2) L−Γ, X–W, K−Γ	2.61
2.68	(v_2-c_2) L−Γ,X–W	2.68
2.73	(v_1-c_1) L−Γ,X−W−K−Γ	2.74
	(v_1-c_2) L−Γ,X−W−K−Γ, W	2.81
3.00	(v_1-c_1) W, W−L−Γ,K−Γ	2.96
	(v_1-c_2) W, W−L−Γ, X–W, K−Γ	2.99,3.03
	(v_2-c_1) L−Γ,X−W−K−Γ	3.03
	(v_2-c_2) L−Γ, X–W, K−Γ	3.00
	(v_2-c_3) L−Γ−X,K−Γ	3.08
3.19	(v_2-c_1) W−L−Γ	3.19
	(v_3-c_2) W, L−Γ−X–W, W, K−Γ	3.17
3.36	(v_3-c_2) L−Γ, W−K−Γ, K	3.33
	(v_2-c_2) W−L−Γ, W−K−Γ, K	3.36
3.55	(v_1-c_3) W−L−Γ, K–X–W, K, X	3.51, 5.53
	(v_2-c_3) W−L−Γ, X−W−K−Γ	3.55
	(v_3-c_1) W−L−Γ, K−Γ	3.52

Table 7
Optical transitions in K_3Sb.

Peak position	Transition	Energy (eV)
2.32	(v_1-c_1) W–L, W, L−Γ, K−Γ	2.34
	(v_2-c_1) L−Γ, X–W, K−Γ	2.32
2.65	(v_1-c_1) W–L, L, K−Γ	2.63
	(v_2-c_1) L, W–K K−Γ	2.65
2.84	(v_2-c_1) W–L, K−Γ,	2.73, 2.80, 2.85
	(v_3-c_1) W, L−Γ, Γ−X, X–W, W–K K−Γ	2.83
2.97	(v_1-c_2) Γ, Γ−X, X–W, K, K–L	3.13
	(v_2-c_1) W–L, K−Γ	3.02
3.22	(v_1-c_2) W–L, L−Γ, X, X−W−K−Γ	3.22
	(v_2-c_3) L−Γ−X, K−Γ	3.21
3.3	(v_1-c_3) L−Γ−X, K−Γ	3.36
	(v_2-c_2) W−L−Γ, X–W, K, K−Γ	3.30
3.65	(v_1-c_3) W, L, Γ−X, K−Γ	3.63, 3.68
	(v_2-c_3) L, Γ−X, K−Γ	3.65
3.76	(v_3-c_1) W–L, L	3.76
4.09	(v_3-c_2) W, W−L−Γ, K−Γ	4.08
4.28	(v_2-c_3) Γ−X−W−K−Γ	4.2
	(v_3-c_3) W−L−Γ	4.39
4.77	(v_3-c_3) L, Γ−X−W−K−Γ	4.74

Table 8
The calculated dielectric constants of the studied compounds. Δ*E* is the energy shift.

Materials	Uncorrected	Corrected	Δ*E* (eV)
Cs_3Sb	9.18	7.5	0.68
Cs_2KSb	8.68		
CsK_2Sb	8.06	7.87	0.07
K_3Sb	8.15	7.42	0.287

bands so as to match the calculated band gaps with the experimental data. In the current study the energy shift is 0.68, 0.07 and 0.287 eV for Cs_3Sb, CsK_2Sb and K_3Sb, respectively. For Cs_2KSb the bandgap has not been measured, to the best of our knowledge. The obtained theoretical values of $\varepsilon(0)$ (with and without shift) are reported in Table 8. Furthermore, one also should add that the present calculations neglect local field [43] and excitonic [50] effects.

3.2.2. The absorption coefficient

The alkali antimonide compounds are very suitable as photoemitters due to their good optical absorption in the visible region of the light spectrum. The absorption coefficient for the studied materials has been calculated in the photon energy range 0–6 eV and they are displayed in Fig. 14. These theoretical spectra are not broadened. It is clear from these spectra that the rate at which the absorption increases with photon energy and the energy at which the absorption becomes relatively constant change from compound to another. Cs_2KSb has the largest rate of absorption increase, a result which has been deduced by Ettema and de Groot [30] from density of states consideration at the bottom of the conduction bands. This compound shows also a strong structure in its absorption above 2 eV with peaks at 2.11 and 2.90 eV and minima at 2.40 and 3.22 eV.

For K_3Sb the absorption coefficient shows also a strong structure in the observed spectrum [2], there is a pronounced peak near 2.4 eV, a minimum near 3.0 eV, and another maximum near 3.4 eV, this is in fairly good agreement with the calculated one.

For Cs_3Sb, the theoretical absorption curve, which is not broadened, compares well in shape with the experimental one [2].

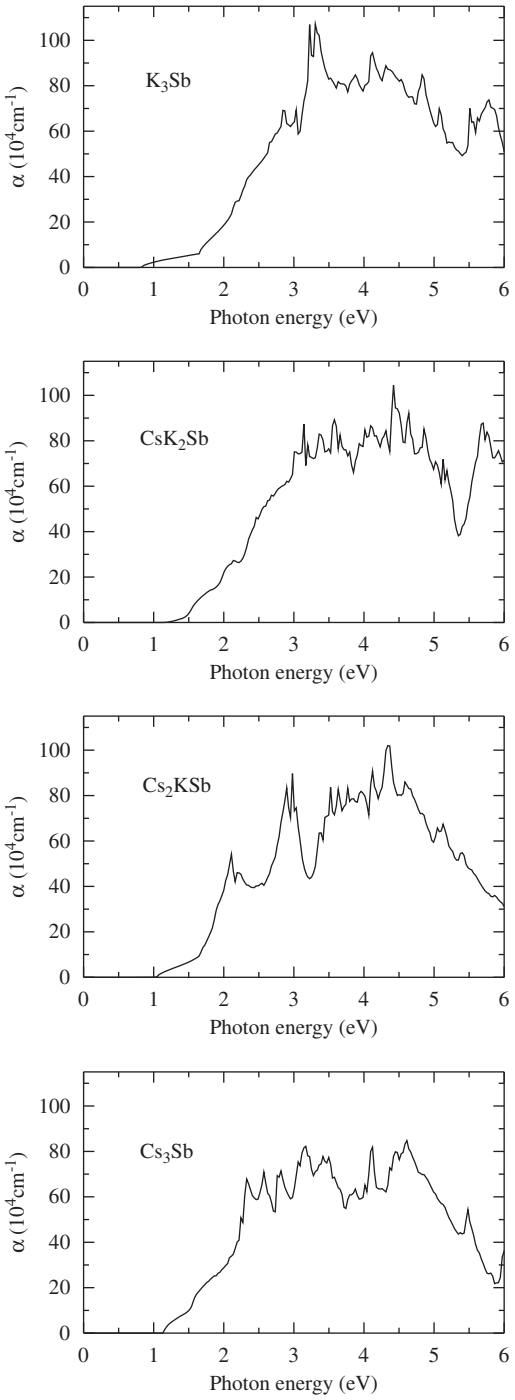

Fig. 14. The absorption coefficient.

4. Conclusion

In conclusion, we have presented first principles study of the optical spectra of the alkali-antimonide compounds Cs_3Sb, Cs_2KSb, CsK_2Sb and K_3Sb. In our calculations the FP-LAPW method in the GGA scheme has been used.

The calculated band structures are in good agreement with previous results. The decomposition of the dielectric functions into individual band-to-band contributions and the plotting of transition band structures allowed to identify the microscopic origin of the features in the optical spectra and the contributions of the different regions in the Brillouin zone. The calculated optical spectra are in good agreement with the available experimental data.

Acknowledgments

One of the authors (B. Bennecer) is very grateful to Professor P. Blaha and his team (Vienna University of Technology, Austria) for providing the wien2k package used in performing this calculation. We thank the Algerian Ministry of Higher Education for financial support for the Project no. D01520070006.

References

[1] W.E. Spicer, Phys. Rev. 112 (1958) 114.
[2] E. Taft, H.R. Philipp, Phys. Rev. 115 (1959) 1583.
[3] W.H. McCarroll, J. Phys. Chem. Solids 22 (1960) 30.
[4] A.H. Sommer, W.E. Spicer, J. Appl. Phys. 32 (1960) 1036.
[5] W.E. Spicer, J. Phys. Chem. Solids 22 (1961) 365.
[6] A.H. Sommer, Appl. Phys. Lett. 3 (1963) 62.
[7] F. Wooten, W.E. Spicer, Surf. Sci. 1 (1964) 367.
[8] W.H. McCarroll, J. Phys. Chem. Solids 26 (1965) 191.
[9] A. Ebina, T. Takahashi, Phys. Rev. B 7 (1973) 4712.
[10] C. Ghosh, B.P. Varma, J. Appl. Phys. 49 (1978) 4549.
[11] C. Ghosh, Phys. Rev. B 22 (1980) 1972.
[12] J. Robertson, Solid State Commun. 47 (1983) 899.
[13] J. Robertson, Phys. Rev. B 27 (1983) 6322.
[14] R.L. Sheffield, E.R. Gray, J.S. Fraser, Nucl. Instrum. Meth. A 272 (1988) 222.
[15] J.M. Barois, C. Fauassier, M. Onillon, B. Tanguy, Mater. Chem. Phys. 24 (1989) 189.
[16] B. Yang, Solid State Electron. 32 (1989) 243.
[17] T. Guo, J. Appl. Phys. 72 (1992) 4384.
[18] M.B. Tzolov, M.N. Iliev, Thin Solid films 213 (1992) 99.
[19] B. Erjavec, Vacuum 45 (1994) 617.
[20] S.H. Kong, J. Kinross-Wright, D.C. Nguyen, R.L. Sheffield, Nucl. Instrum. Meth. A 358 (1995) 617.
[21] T. Guo, Thin Solid films 281 (1996) 379.
[22] P. Michelato, Nucl. Instrum. Meth. A 393 (1997) 455.
[23] A. Breskin, A. Buzulutskov, E. Shefer, R. Chechik, M. Prager, Nucl. Instrum. Meth. A 413 (1998) 275.

[24] E. Shefer, A. Breskin, T. Boutboul, R. Chechik, B.K. Singh, J. Appl. Phys. 92 (2002) 4758.
[25] R. Xiang, Y. Ding, K. Zhao, X. Lu, S. Quan, B. Zhang, L. Wang, S. Huang, L. Lin J. Chen, Nucl. Instrum. Meth. A 528 (2004) 321.
[26] N.E. Christensen, Phys. Rev. B 32 (1985) 207.
[27] S.-H. Wei, A. Zunger, Phys. Rev. B 35 (1987) 3952.
[28] A.R.H.F. Ettema, R.A. de Groot, J. Phys. Condens. Matter 11 (1999) 759.
[29] A.R.H.F. Ettema, R.A. de Groot, Phys. Rev. B 61 (2000) 10035.
[30] A.R.H.F. Ettema, R.A. de Groot, Phys. Rev. B 66 (2002) 115102.
[31] A.R.H.F. Ettema, Appl. Phys. Lett. 82 (2003) 3988.
[32] D. Singh, Planes Waves, Pseudo-potentials and the LAPW Method, Kluwer Academic Publishers, Boston, Dortrecht, London, 1994.
[33] P. Blaha, K. Schwarz, G.K.H. Madsen, D. Kvasnicka, J. Luitz, WIEN2k, An Augmented Plane Wave+Local Orbitals Program for Calculating Crystal Properties, Karlheinz Schwarz, Techn. Universität Wien, Austria, 2001, ISBN 3-9501031-1-2.
[34] Z. Wu, R.E. Cohen, Phys. Rev. B 73 (2006) 235116.
[35] C. Ambrosch–Draxl, J.O. Sofo, Comput. Phys. Commun. 175 (2004) 1.
[36] F.D. Murnaghan, Proc. Natl. Acad. Sci. USA 30 (1944) 244.
[37] L. Hedin, Phys. Rev. 139 (1965) A796.
[38] C.S. Wang, W.E. Pickett, Phys. Rev. Lett. 51 (1983) 597.
[39] W.E. Pickett, C.S. Wang, Phys. Rev. B 30 (1984) 4719.
[40] B. Arnaud, M. Alouani, Phys. Rev. B 62 (2000) 4464.
[41] B. Arnaud, M. Alouani, Phys. Rev. B 63 (2001) 085208.
[42] S. Lebegue, B. Arnaud, M. Alouani, P.E. Bloechl, Phys. Rev. B 67 (2003) 155208.
[43] S. Lebegue, M. Alouani, Phys. Rev. B 72 (2005) 085103.
[44] M. Alouani, L. Brey, N.E. Christensen, Phys. Rev. B 37 (1988) 1167.
[45] I. Gorezyca, N.E. Christensen, M. Alouani, Phys. Rev. B 39 (1989) 7705.
[46] N.E. Christensen, I. Gorezyca, Phys. Rev. B 50 (1994) 4397.
[47] W.R.L. Lambrecht, S.N. Rashkeev, Phys. Status Solidi (b) 217 (2000) 599.
[48] F. Kootstra, P.L. de Boeij, J.G. Snijders, Phys. Rev. B 62 (2000) 7071.
[49] C. Persson, R. Ahuja, A. Ferreira da Silva, B. Johansson, J. Phys. Condens. Matter (2001) 138945.
[50] R. Laskowski, N.E. Christensen, Phys. Rev. B 73 (2006) 045201 and references therein.